# Effect of Helical Flanking Sequences on the Morphology of Polyglutamine-Containing Fibrils

Bashkim Kokona, Karl A. Johnson, and Robert Fairman*

Department of Biology, Haverford College, 370 Lancaster Avenue, Haverford, Pennsylvania 19041, United States

**Ⓢ** *Supporting Information*

**ABSTRACT:** A peptide model system has been developed to study the effects of helical flanking sequences on polyglutamine aggregation. In a companion manuscript, the kinetics of aggregation are described, comparing the influence of a well-defined heterotetrameric coiled coil to that of the helix-rich structure found in Htt$^{NT}$, a 17-residue flanking sequence found in the huntingtin protein, on polyglutamine aggregation. Here, the morphological characterization of the resultant fibrils that form for a set of peptides is reported, only one of which, KKQ$_{25}$KK, has been previously studied. A careful analysis of TEM and AFM images of KKQ$_{25}$KK confirms that it forms bundled fibrils of varying length and reveals, unexpectedly, that they are composed of fully extended cross-$\beta$-strands. Second, it is shown that helical flanking sequences do not disrupt the assembly of a core cross-$\beta$-sheet structure, but such flanking sequences can influence higher order processes, such as inhibiting the bundling of the fibrils.

Polyglutamine aggregation is a hallmark of at least 12 human neurodegenerative diseases, including Huntington's disease and a set of spinocerebellar ataxias.[1] The underlying secondary structure in the aggregated material is thought to be cross-$\beta$-sheet, which can extend in directions orthogonal to the strand geometry due to backbone hydrogen bonding[2] and in directions lateral to the sheets themselves through glutamine side-chain interactions (often referred to as lamination).[3] Higher order bundling of such fibrils has also been observed.[4] General elements of the assembly and morphology of polyglutamine aggregates have been largely elucidated,[1] and more recently, the influence of flanking sequences on the assembly pathway has been studied intensively (including our accompanying paper[28]).[5,6] In contrast, there is only limited information available on how flanking sequences influence higher order structure and general fibrillar morphology. However, there is some suggestion that the core cross-$\beta$-sheet structure is unperturbed based on ssNMR[7] and FTIR data.[5] Interestingly, flanking sequences derived from the huntingtin N-terminal domain result in some branching and general thickening of fibrils, but with less overall higher order bundling.[1] Exploring the role of such flanking domains on the structure of polyglutamine aggregates is a central aim of the work that is described here. In particular, exploring sequence/structure relationships in helical-rich domains such as that seen in the huntingtin N-terminal domain may offer insights into mitigating polyglutamine aggregation.[8,9]

Our accompanying paper[28] focuses on the influence of a designed helical domain on the assembly process of polyglutamine fibrils. A more extensive review of the literature will be found in the Introduction section of this accompanying manuscript, and the introductory remarks are restricted here to those that most directly support our experimental approach.

The same designed helical domain is used to explore the effects of such flanking sequences on the larger scale morphologies of polyglutamine fibrils. The questions that are explored include the extent to which flanking sequences affect (1) the core cross-$\beta$-sheet structure, (2) fibrillar length, (3) lateral assembly, (4) bundling, and (5) general heterogeneity. Such efforts may reveal mechanistic details of higher order aggregation and thus allow for new approaches to the design of inhibitors of polyglutamine aggregation. The helical domain sequence is based on our previous work exploring the role of salt bridge interactions in stabilizing a parallel heterotetrameric coiled coil.[10] The sequence contains lysines at all "e" and "c" heptad positions (ecK) and can form homotetramers under appropriate salt or pH conditions. The accompanying work[28] shows that the fusion of the lysine-rich helical domain inhibits polyglutamine aggregation (with and without an intervening "linker" sequence, designed to introduce a helix stop signal) and suggests that this is, in large part, due to a repulsive charge effect. Nevertheless, aggregation does occur and thus it was intriguing to characterize the resultant aggregates, using both AFM and TEM methodologies.

## ■ MATERIALS AND METHODS

**Peptide Synthesis and Purification.** The peptides used in this study, KKQ$_{25}$KK, ecKQ$_{25}$KK, and ecK-Ω-Q$_{25}$KK, were

purchased from Yale University, Keck Biotechnology Center (see the Figure 1 caption for peptide sequences). Crude peptides were purified as described in the accompanying work.[28] In brief, they were purified using reversed-phase high-performance liquid chromatography (RP-HPLC) with a mobile phase of water and acetonitrile with 0.1% TFA on a Varian ProStar system equipped with a Varian Dynamax semi-preparative C18 column. Peptide identities were confirmed using MALDI-TOF mass spectrometry, yielding the following molecular masses (in daltons, reported as experimental; theoretical): $KKQ_{25}KK$ (3734.6; 3734.0), $ecKQ_{25}KK$ (6904.6; 6903.0), and $ecK-\Omega-Q_{25}KK$ (7425.1; 7425.5).

**Disaggregation and Fibril Preparation Protocols.** Peptides were disaggregated as described in our accompanying work,[28] using a modified version of the protocol developed by the Wetzel lab.[11] In brief, 2 to 3 mg of lyophilized peptide was dissolved and incubated in a mixture of 1:1 HFIP/TFA. After 16 h, the solutions were evaporated and thoroughly dried. Dried samples were dissolved in $H_2O$/0.1% TFA and filtered through a 0.2 $\mu$m low-protein-binding filter. Samples were then centrifuged at 50 000 rpm at 4 °C for 6 h. After this centrifugation step, the top ∼60% of the supernatant was removed. Protein stock solutions were again filtered through a 0.2 $\mu$m low-protein-binding filter. Stock concentrations were determined using either a modified ninhydrin assay[12,13] or by measuring tyrosine absorbance at 280 nm in 6 M GuHCl.[14] Final concentrations of the peptide stocks were in the range of 215−230 $\mu$M.

Generally, fibrils were prepared using a protocol developed by the Wetzel laboratory,[4] in 2.7 mM KCl, 136.9 mM NaCl, 1.5 mM potassium phosphate, 8.9 mM sodium phosphate, pH 7.1 (PBS, pH 7.1), and matured at 37 °C with gentle shaking. Fibrils of $KKQ_{25}KK$ were similar in morphology to that seen in the microscopy images in Figure 2 from Kar et al.[4]

**Fourier Transform Infrared Spectroscopy.** Samples for FTIR analysis were prepared in PBS, pH 7.1. Peptide samples were matured for 14 days, and then 5 $\mu$L of the sample was spotted on a $CaF_2$ window and air-dried. FTIR spectra were collected using a Vertex 70 instrument (Bruker Optics, The Woodland, TX) equipped with Opus version 5.5 software. Spectra were collected at room temperature in the range of 900−4000 $cm^{-1}$, using a resolution of 2 $cm^{-1}$ and averaging a total of 512 scans. Second-order derivative analysis of FTIR spectra was performed using Origin v. 8.6, without smoothing.

**Transmission Electron Microscopy.** For TEM, samples prepared as described above were applied to glow-discharged, Formvar/carbon-coated 300 mesh Cu grids (Electron Microscopy Sciences, Hatfield, PA). After several minutes, the grids were washed with three drops of ultrapure water, followed by three drops of 4% phosphotungstic acid (EMS, pH 7.2 with NaOH) or 2% uranyl acetate (EMS). Excess liquid was wicked from the grid at each step using filter paper, and following the last drop of stain, samples were air-dried. The grids were examined on a JEM-1400 electron microscope (JEOL, Peabody, MA) operated at 100 kV and equipped with an Orius 832 CCD camera (Gatan, Warrendale, PA). Images were acquired using Gatan's Digital Micrograph software and were cropped and assembled using Photoshop (Adobe, San Jose, CA).

**Atomic Force Microscopy.** Peptide samples were prepared using PBS, pH 7.1, and matured up to 14 days; 10 $\mu$L aliquots were removed at days 9 and 14 for deposition onto freshly cleaved mica (Asheville-Schoonmaker Mica Co., New-

port News, VA). The mica with the deposited peptide fibrils was then washed three times for 2 min each with Milli-Q-purified water and dried using high purity $N_2$. Additional aliquots were flash-frozen in liquid $N_2$ and stored in −80 °C for TEM experiments. Samples were imaged in tapping mode using a Nanoscope III AFM (Digital Instruments, Santa Barbara, CA). High-frequency cantilevers (Budget Sensor Multi 75Al-G with 30 nm thick aluminum reflex coating, force constant 3 N/m, nominal curvature <10 nm, resonance frequency 75 ± 15 kHz) were used for all AFM measurements.

**Image Processing.** AFM images converted to a linear gray scale color table were transferred from the Nanoscope III software environment to Sigma Pro (v. 5.0; SSI, San Jose, CA) for further analysis. The 8-bit grayscale 512 × 512 pixel images were then calibrated using the known in-plane scale distances. Images to be analyzed were first smoothed or flattened by subtracting the background intensity to correct for surface effects. The intensities were then calibrated using known AFM z-axis dimensions, defined as perpendicular to the imaging plane. Heights were analyzed by tracing along the filament axes, and data were transferred to Origin (v. 8.6 Origin Lab, Northampton, MA) to perform statistical analysis and fitting. For the height measurements, frequency counts were binned at 0.5 nm intervals from 3 to 11 nm, and plotted histograms were fitted to a single-Gaussian distribution. Height measurements were confirmed by performing several manual cross sections of the fibrils using a Nanoscope III (Digital Instruments, Santa Barbara, CA). Transmission electron microscope images were analyzed using ImageJ (v. 1.47; Wayne Rasband, National Institutes of Health, Bethesda, MD).

## ■ RESULTS

**$KKQ_{25}KK$.** The goal of the work described here is to establish the role of helix-rich domains in the assembly and mesoscale structure of polyglutamine aggregates. The characterization of the effects of such flanking domains on the kinetics and mechanism of assembly is explored in the accompanying paper.[28] In this article, the focus is on how our tetrameric coiled-coil model system[10] affects the morphology of fibrils that are formed from a 25-residue polyglutamine sequence and to compare this to the morphology that is observed for $KKQ_{25}KK$. First, the basic morphological features of $KKQ_{25}KK$ are confirmed by comparison to earlier work,[4] and the structural characteristics are then explored in greater detail.

The $KKQ_{25}KK$ peptide was disaggregated as described in Materials and Methods and prepared in PBS, pH 7.1. Fibrils were matured at 37 °C with gentle shaking for various lengths of time consistent with that reported earlier.[4] To ascertain the secondary structure in these matured fibrils, FTIR measurements were made after drying of matured fibrils on a $CaF_2$ window (Figure 1). The amide I band is clearly evident at 1625.7 $cm^{-1}$, consistent with the expected C=O stretch of the backbone amide bond as found in a $\beta$-sheet conformation.[15] A weak secondary amide I band is observed at 1684.5 $cm^{-1}$, which is often seen with aggregated cross-$\beta$-sheets.[16] The other prominent bands, at 1604.0 and 1657.5 $cm^{-1}$, represent the N−H and C=O vibrational frequencies, respectively, associated with the glutamine side-chain amide groups.[15] These findings are consistent with those published on the same peptide by Kar et al.[4] and other measures of the $\beta$-sheet conformation in fibrils, such as binding of the amyloid dyes, ThT, and DCVJ (see also our accompanying manuscript[28]).[17,18]
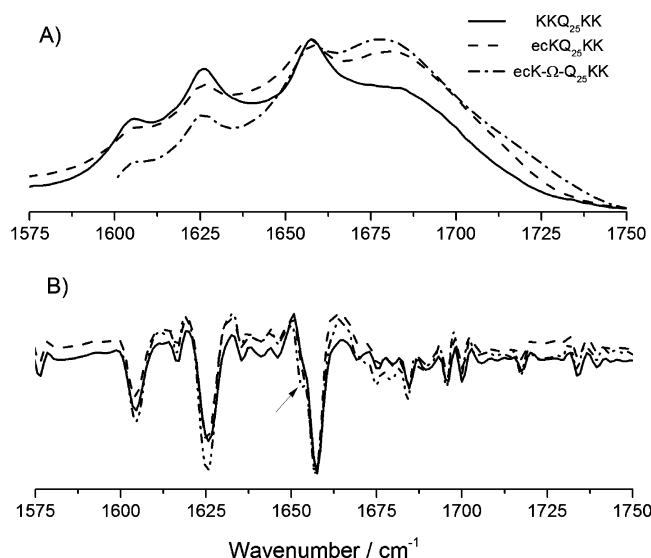
**Figure 1.** FTIR spectra of 140 $\mu$M each of KKQ$_{25}$KK, ecKQ$_{25}$KK, and ecK-$\Omega$-Q$_{25}$KK 14 day old fibrils grown at 37 °C under constant shaking. (A) Absorbance spectra in the amide I region. (B) Second derivative of the absorption spectra. Band assignments: 1604.5 cm$^{-1}$, Gln side-chain N−H; 1625.7 cm$^{-1}$, amide I C=O (extended conformation); 1657.5 cm$^{-1}$, Gln side-chain C=O; 1653.2 cm$^{-1}$, amide I C=O (in helical conformation, band is highlighted with an arrow); 1684.5 cm$^{-1}$, amide I C=O (extended conformation, secondary). ecKQ$_{25}$KK: MKKIKDKLEKIKSKLYKIKNELAKIKKL QQQQQQQQQQQQQQQQQQQQQQQQQKK. ecK-$\Omega$-Q$_{25}$KK: MKKIKDKLEKIKSKLYKIKNELAKIKKL GGSPGGS QQQQ-QQQQQQQQQQQQQQQQQQQQQKK.



**Figure 2.** Images of KKQ$_{25}$KK fibrils prepared at 140 $\mu$M concentration and matured for 14 days in PBS, pH 7.1, at 37 °C prior to deposition. (A) TEM image using PTA negative staining. Scale bar = 100 nm. (B) AFM image. Scale bar = 500 nm. (C) AFM image showing region of low density used for height analysis. Scale bar = 100 nm. (D) Histogram of height analysis (data reported in Table 2).

TEM and AFM imaging was used to study the morphological features of the KKQ$_{25}$KK fibrils in greater detail. Not surprisingly, the morphology of the KKQ$_{25}$KK fibrils imaged using TEM (Figure 2A) looks quite similar to that observed for the same peptide by Wetzel's laboratory (see Figure 2n in Kar et al.).[4] Minor differences in the overall contrast and sharpness of the images are likely due to our use of PTA stain as opposed to the use of UA as a stain[4] (see also Figure S1 in the Supporting Information for representative UA staining of KKQ$_{25}$KK). Features of note that are in common with previous work include evidence of limited bundling (approximately 5 fibrils per bundle), a certain degree of entanglement of the bundles, and lengths in the range of 200−300 nm for the smaller bundles (Table 1). Evidence for bundles are seen in the micron range, which had not been shown previously.[4] Individual fibril widths were estimated roughly by determining the width of clearly isolated bundles and then dividing appropriately by the number of striations in the bundles (Table 2). The width of 6.8 ± 0.8 nm is too large to be consistent with the dimensions of a hairpin structure,[19] suggesting that the units of assembly likely represent extended $\beta$-strands. This possibility was explored more carefully through a quantitative analysis of the AFM images that were collected for this peptide.

AFM images of KKQ$_{25}$KK fibrils also show fibril bundling (Figure 2B), with striations clearly delineating individual fibrils. The average length of the bundles also appears to be consistent with that seen in the TEM images. Most of the clearly defined bundles fall in the range of 200−300 nm, with some extending out to about 600 nm (Table 1). In addition to the bundles, there appear to be much shorter individual fibrils, which are
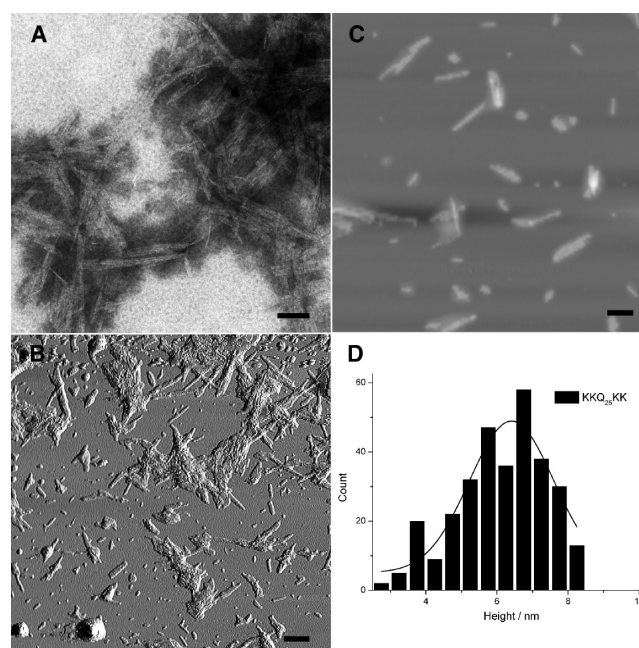
## Table 1. Peptide Fibril Lengths

| peptide | AFM measurements[a] | | TEM measurements[b] | |
|---|---|---|---|---|
| | length (nm) | range | length (nm) | range |
| KKQ$_{25}$KK | 65.5 | 22.2−141 | | |
| ecKQ$_{25}$KK | 104.0 | 17.4−210 | 94.1 | 29.1−186 |
| ecK-$\Omega$-Q$_{25}$KK | 82.0 | 28.0−243 | 126.2 | 54.3−329 |

[a]AFM measurements are made using images in Figure 2C for KKQ$_{25}$KK, Figure 5A for ecKQ$_{25}$KK, and Figure 5D for ecK-$\Omega$-Q$_{25}$KK. [b]TEM measurements made using images in Figure 3A for ecKQ$_{25}$KK and Figure 3C for ecK-$\Omega$-Q$_{25}$KK.

## Table 2. Peptide Fibril Heights and Widths

| peptide | height (nm)[a] | TEM width (nm)[b] |
|---|---|---|
| KKQ$_{25}$KK | 9.1 ± 0.2 | 6.8 ± 0.8 |
| ecKQ$_{25}$KK | 9.7 ± 0.1 | 8.9 ± 1.3 |
| ecK-$\Omega$-Q$_{25}$KK | 7.8 ± 0.1 | 9.7 ± 1.3 |

[a]AFM measurements are made using images in Figure 2C for KKQ$_{25}$KK, Figure 5A for ecKQ$_{25}$KK, and Figure 5D for ecK-$\Omega$-Q$_{25}$KK and have a 30% correction factor applied.[20] [b]TEM measurements are made using images in Figure 2A for KKQ$_{25}$KK, Figure 3A for ecKQ$_{25}$KK, and Figure 3C for ecK-$\Omega$-Q$_{25}$KK.

more clearly seen in areas of lower deposition density (Figures 2C and S2 in the Supporting Information). Such fibrils have lengths ranging in between 22 and 140 nm (Table 1). The shorter lengths of the individual fibrils may be a result of mechanical disruption of the larger scale structures during sample preparation.

The individual fibrils in Figure 2C were analyzed to determine their heights, and a histogram of binned data is shown in Figure 2D. This histogram appears to be well-fitted to

a single-Gaussian distribution, with a peak centered at 6.41 ± 0.14 nm. Combining the analysis across the images in both Figures 2C and S2, the heights are approximately the same, with a value of 6.59 ± 0.11 nm. Experimentally determined heights in AFM experiments typically are smaller than the actual heights of protein structures due to the compressibility of proteins in response to tapping of the type of high-frequency cantilever that was used. Accounting for a 30% height correction for the data presented in Figure 2,[19−22] the KKQ$_{25}$KK fibrils should have an average height of about 9.1 nm (Table 2). This average height is quite consistent with the width of a cross-$\beta$-strand fibril made up of fully extended 24-residue chains (rather than chains adopting hairpin motifs). It is formally possible that this height is instead reflective of varying degrees of $\beta$-sheet lamination. If one assumes a 2.0 nm thickness for a bilayer of $\beta$-sheets,[19] then this would suggest a heterogeneity of lamination ranging from 4 to 8 sheets. This was ruled out simply because the features of the fibrils in both the TEM and AFM images are too regular to support such a conclusion.

It is intriguing to note that the TEM widths and AFM heights of individual fibrils are roughly the same. This may simply be due to differential modes of binding to the surfaces that are used for TEM and AFM work. For the AFM samples, the heights would reflect the lengths of the individual strands extended orthogonally with respect to the plane of the mica, presenting the end lysine residues as the primary points of contact. In contrast, these same extended strands would be parallel to the Formvar/carbon-coated surface of the copper grids, with the lysines and the glutamines simultaneously engaged in surface binding. This variation in surface-dependent deposition orientation of cross-$\beta$-strand fibrils has been observed by others.[23] The morphological features described here for KKQ$_{25}$KK will be compared to related features identified for ecK-$\Omega$-Q$_{25}$KK in the Discussion section.

**ecKQ$_{25}$KK and ecK-$\Omega$-Q$_{25}$KK.** As described above, an unexpected feature (e.g., extended rather hairpin conformations of the individual strands) in the KKQ$_{25}$KK aggregation beyond that described earlier in the literature was noted, and it was of interest to determine whether this same feature would be present in fibrils formed in our two coiled-coil fusion constructs. Polymers formed from the coiled-coil fusion constructs were examined for unique features that might provide insight into the aggregation mechanism.

First, as was done with KKQ$_{25}$KK, FTIR measurements were carried out on samples of ecKQ$_{25}$KK and ecK-$\Omega$-Q$_{25}$KK after maturation to form fibrils (Figure 1). The ecKQ$_{25}$KK FTIR spectrum is similar to that of KKQ$_{25}$KK with major and minor amide I bands at 1625.7 and 1684.5 cm$^{-1}$, suggesting that the $\beta$-sheet conformation dominates the structure. Likewise, the other prominent bands at 1657.5 and 1604.5 cm$^{-1}$ correspond to the glutamine C=O stretch and the N−H bend. In ecK-$\Omega$-Q$_{25}$KK, in addition to the bands observed for ecKQ$_{25}$KK, a shoulder at 1653.2 cm$^{-1}$ appears more prominently (arrow in Figure 1), suggesting some evidence for a helical conformation, perhaps due to residual helical structure in the ecK sequence. Evidence for the dominance of the $\beta$-sheet conformation in these peptides in solution is further supported by circular dichroism solution studies, as shown in the accompanying work.[28]

Given the complexity of the aggregation assembly processes that were observed for the ecKQ$_{25}$KK and ecK-$\Omega$-Q$_{25}$KK fusion peptides (accompanying paper[28]), the morphology at various

time points during the fibril maturation process was explored, using both TEM and AFM methods. The question that was addressed is whether the coiled-coil motif plays an integral role in the fibrillar morphology, either through influencing the cross-$\beta$-sheet structure or some feature of the higher order structure. TEM images were collected at 9 and 14 days of maturation for both peptides (Figure 3), with the times chosen
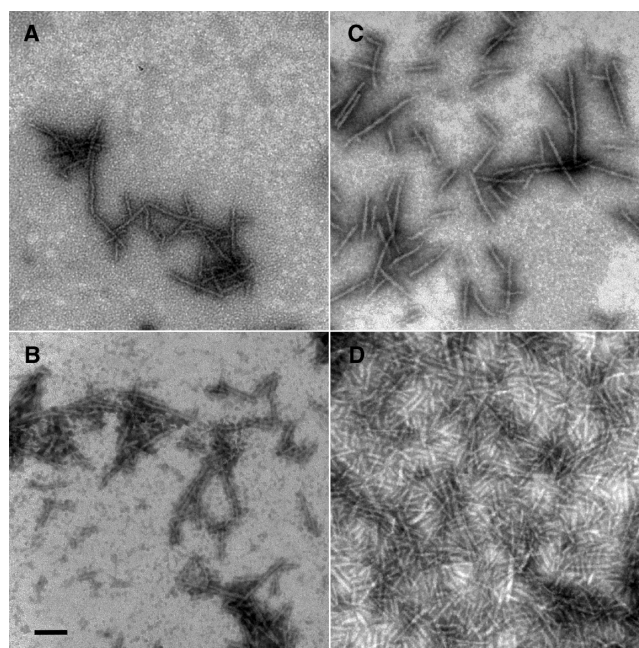


**Figure 3.** TEM images of polyglutamine fibrils at different maturation times. (A) ecKQ$_{25}$KK fibrils prepared at 140 $\mu$M monomer concentration and matured for 9 days; (B) ecKQ$_{25}$KK fibrils prepared at 140 $\mu$M monomer concentration and matured for 14 days; (C) ecK-$\Omega$-Q$_{25}$KK fibrils prepared at 140 $\mu$M monomer concentration and matured for 9 days; and (D) ecK-$\Omega$-Q$_{25}$KK fibrils prepared at 140 $\mu$M monomer concentration and matured for 14 days. All samples were incubated at 37 °C in PBS, pH 7.1. PTA negative staining was used for all deposited samples. The scale bar shown in panel B represents 100 nm and is the same for all panels.

to represent early onset of aggregation and near completion of aggregation, respectively. In contrast to the KKQ$_{25}$KK images, no evidence of bundling of the fibrils was seen. A likely explanation for lack of bundling is charge repulsion among the 12 lysine residues in the helical domain. This lack of bundling provides an opportunity to characterize the fibrils themselves, and the average lengths (Table 1) and widths (Table 2) measured using these images are only slightly larger than those seen for the KKQ$_{25}$KK peptide. It is perhaps not surprising that the widths are somewhat larger since the ecK pendant groups would be expected to add somewhat to this dimension. Thus, it was concluded that the ecK addition in either peptide is not integrally involved in the core fibril architecture, suggesting that the helical domains decorate the edges of the ribbon structure in the polymer.

Closer examination of the TEM images for ecKQ$_{25}$KK and ecK-$\Omega$-Q$_{25}$KK revealed a unique feature not seen in the KKQ$_{25}$KK images (Figure 4). In both peptides, a spine of lighter staining intensity running along the core of the polymer was noted, most clearly seen for the ecK-$\Omega$-Q$_{25}$KK peptide (white arrows, Figure 4B). It is likely that this spine represents the cross-$\beta$-strand part of the structure, with the more weakly
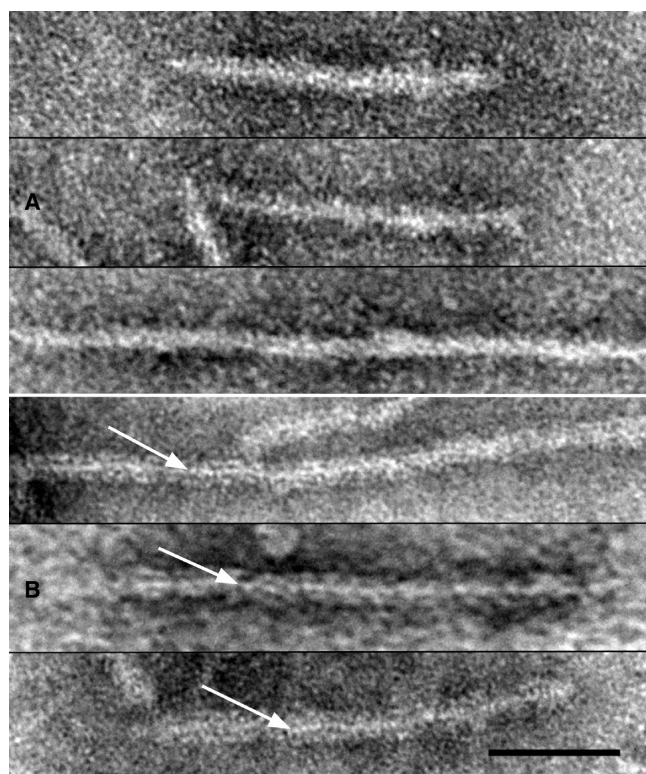
**Figure 4.** High-magnification TEM images of ecKQ$_{25}$KK and ecK-Ω-Q$_{25}$KK. The same samples shown in Figure 3 were reimaged at higher magnification in order to reveal additional features. The top three examples (A) show images of ecKQ$_{25}$KK fibrils. The bottom three examples (B) show images of ecK-Ω-Q$_{25}$KK fibrils, and the white arrows denote a core structure visible along each fibril. The scale bar shown in the bottom panel of B represents 50 nm and is the same for all images.



**Figure 5.** Tapping mode AFM images of ecKQ$_{25}$KK and ecK-Ω-Q$_{25}$KK fibrils prepared at 140 $\mu$M concentration in PBS, pH 7.1, at 37 °C prior to deposition. (A) Image of ecKQ$_{25}$KK fibrils matured for 9 days. (B) Image of ecKQ$_{25}$KK fibrils matured for 14 days. (C) Overlay of histogram height analyses of KKQ$_{25}$KK (taken from Figure 2D) and ecKQ$_{25}$KK (image C). (D) Image of ecK-Ω-Q$_{25}$KK fibrils matured for 9 days. (E) Image of ecK-Ω-Q$_{25}$KK fibrils matured for 14 days. (F) Overlay of histogram height analyses of KKQ$_{25}$KK (taken from Figure 2D) and ecK-Ω-Q$_{25}$KK (image D). The scale bar shown in panel A represents 100 nm and is the same for all images shown in this figure.

stained outer edge features representing the N-terminal flanking domains (more clearly observed for ecK-Ω-Q$_{25}$KK, containing the intervening linker sequence).

The fibrils for ecKQ$_{25}$KK and ecK-Ω-Q$_{25}$KK were also imaged using AFM (Figure 5). The main difference in samples matured for 9 days (Figure 5A,D) versus 14 days (Figure 5B,E) seems to be in the quantity of fibrils seen in the images, as no other discernible differences are evident. The fibrils for both peptides are quite heterogeneous in length, ranging from about 20 to 240 nm (Table 1), and are similar in distribution to that observed in the TEM images (Figure 3A,C). Height analyses of the fibrils are shown for both peptides as a set of histograms (Figure 5C,F and Table 2) using the images from Figure 5A,D. On the basis of single-Gaussian fits, fibril heights for ecKQ$_{25}$KK average at 9.7 nm after tip compression correction, consistent again with the expected height for a fully extended cross-$\beta$-strand structure. In contrast, the height measured for ecK-Ω-Q$_{25}$KK (Figure 5F) was somewhat smaller, with an average tip compression-corrected height of 7.8 nm.

## ■ DISCUSSION

In the process of calibrating this work against previously published studies on KKQ$_{25}$KK,[4] the characterization of the cross-$\beta$-sheet fibrillar morphology revealed additional details. Careful analysis of the AFM and TEM images reveal an unexpected feature involving an extended strand conformation within the cross-$\beta$-sheet core. The predicted extended
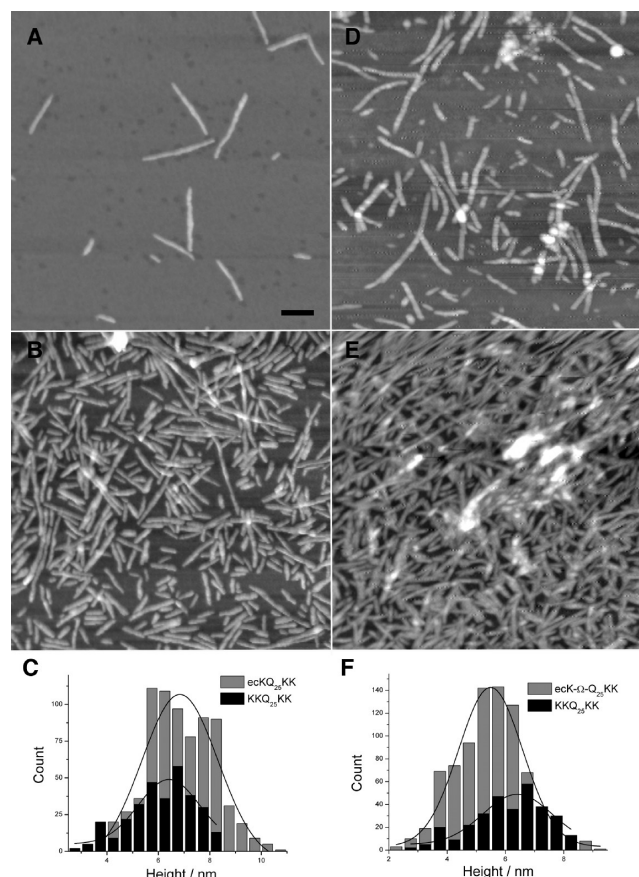
conformation for the chains in the fibrils surprised us since an obvious nucleation intermediate for early polyglutamine assembly could have been a monomeric hairpin structure.[4] Assuming an extended structure in the cross-$\beta$-fibril, it is more likely that the nucleation intermediate represents two extended chains held together via backbone hydrogen bonding along with some likely desolvation of the glutamine side chains; such a two-chain nucleation intermediate has been proposed for this sequence.[4] Although there are only limited examples of quantitative analysis of polyglutamine fibril widths, the widths appear to be restricted to between 5 and 9 nm regardless of the absolute number of glutamine residues (Table 3). A restriction to this width suggests that turns become favorable beyond approximately 20–25 glutamine residues in strand length, suggesting that the cost of forming a turn must be energetically compensated through the backbone and side-chain interactions formed within the resultant hairpin; this is supported by work from Wetzel's laboratory that suggests polyQ sequences that are 26 residues or longer nucleate through a monomeric intermediate, most likely due to stable hairpin formation.[4] Other work from the Wetzel laboratory, in which Pro-Gly is inserted into polyglutamine sequences, results in rapid

**Table 3. Comparison of Fibril Widths with Literature Values**

| peptide | theoretical width (nm)[a] | measured width (nm) | no. of residues per strand[b] | predicted no. of strands[c] |
|---|---|---|---|---|
| $D_2Q_{15}K_2$[d] | 6.5[c] | 7–8 | 20–23 | 1 |
| $KKQ_{25}KK$ | 9.9 | 9.1 | 27 | 1 |
| $KKQ_{32}KK$[e] | 12.2 | 5–7 | 15–20 | 2 |
| $GK_2Q_{38}K_2$[d] | 14.6 | 7–8 | 20–23 | 2 |
| $GK_2Q_{54}K_2$[d] | 20.1 | 7–8 | 20–23 | 3 |
| $ecKQ_{25}KK$ | 18.7 | 9.7 | 28 | 1 |
| $ecK-\Omega-Q_{25}KK$ | 21.1 | 7.8 | 23 | 1 |

[a]Calculated assuming an extended peptide conformation. [b]Calculated by dividing the measured length by 0.34 nm. [c]Estimated by comparing the calculated number of residues per strand with the actual peptide sequence length (excluding helical domains). [d]Data taken from ref 27. [e]Data taken from ref 6.

aggregation for strands containing 9 or 10 glutamines each, and this shorter length of glutamines is perhaps not surprising since Pro-Gly would help to stabilize the turn more than a glutamine pair would.[24]

In sum, our detailed image analysis of fibril morphology for our set of peptides, as measured by both TEM and AFM, show that addition of an N-terminal helical domain does not disrupt the formation of cross-$\beta$-sheet structures but that it does result in a significant inhibition of fibril bundling. This effect can most likely be ascribed to unfavorable electrostatic interactions among the lysine residues found in the helical domain. Our work provides further evidence that cross-$\beta$-sheet assembly can be robust to flanking sequence effects, whereas their influence suggests significant plasticity in higher order fibrillar morphologies, a paradigm that appears to be emerging in recent work on other aggregating systems.[25]

The results from this work, and of the accompanying paper,[28] encouraged us to propose a model for possible modes of assembly (Figure S3 in Supporting Information) that is similar to that proposed by Wetzel and his colleagues based on work using an Htt[NT] construct.[1] While helix formation (structure B in Figure S3) leading to coiled-coil assembly (structure C) is similar to what has been proposed by Wetzel and his colleagues, in our case, the structure is limited to an oligomeric state of four. This structure (structure C) would be a site for nucleation of $\beta$-strands that would then act as a template for further addition of tetramers to form an extended $\beta$-sheet polymer. Since our highly charged helical sequences appear to inhibit aggregation, the more favorable nucleation (structure B) is likely instead to involve the interaction of two extended strands in the absence of helical interactions to form a two-stranded $\beta$-sheet. This can then act as a template for further growth through subunit addition. It is important to distinguish the nucleation intermediate for initial assembly events (as we describe above and as described by others[1]) from other more stable intermediate structures that might be involved in either on or off pathway assemblies.[6,26] The precise role of such higher order oligomeric stable states remains unresolved and of intense interest.

On the basis of the results presented here, the coiled-coil domains appear to decorate the edges of the core structure, thus not influencing the overall morphology of the fibrils, with the exception of the inhibition of fibril bundling. How these higher order morphologies relate to cytotoxicity and disease is still poorly understood, but our model system suggests that interventions can be designed to favor different morphologies,

and these favored conformations can then be assessed on cells and in animal model systems. For example, it has been shown that doping the huntingtin aggregation process with designed helix-rich peptides can influence assembly and morphology,[8,9] so perhaps the presence of highly charged helix-rich peptides might not only inhibit the kinetics of huntingtin aggregation but also limit the degree of aggregation.

## ■ ASSOCIATED CONTENT

**Ⓢ Supporting Information**

TEM images of $ecKQ_{25}KK$ and $ecK-\Omega-Q_{25}KK$ fibrils stained using uranyl acetate (Figure S1), AFM image of $KKQ_{25}KK$ (Figure S2), and proposed model for $ecKQ_{25}KK$ aggregation (Figure S3). This material is available free of charge via the Internet at http://pubs.acs.org.

## ■ AUTHOR INFORMATION

**Corresponding Author**

*Tel.: (610) 896-4205; Fax: (610) 896-4963; E-mail: rfairman@haverford.edu.

## ■ ACKNOWLEDGMENTS

## ■ ABBREVIATIONS

AFM, atomic force microscopy; FTIR, Fourier transform infrared spectroscopy; HFIP, 1,1,1,3,3,3-hexafluoro-2-propanol; MALDI-TOF, matrix assisted laser desorption/ionization-time-of-flight; PTA, phosphotungstic acid; RP-HPLC, reversed-phase high-performance liquid chromatography; TEM, transmission electron microscopy; TFA, trifluoroacetic acid; UA, uranyl acetate; $\Omega$, GGSPGGS linker sequence

## ■ REFERENCES

(1) Wetzel, R. (2012) Physical chemistry of polyglutamine: intriguing tales of a monotonous sequence. *J. Mol. Biol. 421*, 466–490.

(2) Dobson, C. M. (2001) The structural basis of protein folding and its links with human disease. *Philos. Trans. R. Soc., B 356*, 133–145.

(3) Sikorski, P., and Atkins, E. (2005) New model for crystalline polyglutamine assemblies and their connection with amyloid fibrils. *Biomacromolecules 6*, 425–432.

(4) Kar, K., Jayaraman, M., Sahoo, B., Kodali, R., and Wetzel, R. (2011) Critical nucleus size for disease-related polyglutamine aggregation is repeat-length dependent. *Nat. Struct. Mol. Biol. 18*, 328–336.

(5) Thakur, A. K., Jayaraman, M., Mishra, R., Thakur, M., Chellgren, V. M., Byeon, I. J., Anjum, D. H., Kodali, R., Creamer, T. P., Conway, J. F., Gronenborn, A. M., and Wetzel, R. (2009) Polyglutamine disruption of the huntingtin exon 1 N terminus triggers a complex aggregation mechanism. *Nat. Struct. Mol. Biol. 16*, 380–389.

(6) Legleiter, J., Mitchell, E., Lotz, G. P., Sapp, E., Ng, C., DiFiglia, M., Thompson, L. M., and Muchowski, P. J. (2010) Mutant huntingtin

fragments form oligomers in a polyglutamine length-dependent manner *in vitro* and *in vivo*. *J. Biol. Chem.* 285, 14777−14790.

(7) Sivanandam, V. N., Jayaraman, M., Hoop, C. L., Kodali, R., Wetzel, R., and van der Wel, P. C. A. (2011) The aggregation-enhancing huntingtin N-terminus is helical in amyloid fibrils. *J. Am. Chem. Soc.* 133, 4558−4566.

(8) Mishra, R., Jayaraman, M., Roland, B. P., Landrum, E., Fullam, T., Kodali, R., Thakur, A. K., Arduini, I., and Wetzel, R. (2012) Inhibiting the nucleation of amyloid structure in a huntingtin fragment by targeting alpha-helix-rich oligomeric intermediates. *J. Mol. Biol.* 415, 900−917.

(9) Jayaraman, M., Mishra, R., Kodali, R., Thakur, A. K., Koharudin, L. M., Gronenborn, A. M., and Wetzel, R. (2012) Kinetically competing huntingtin aggregation pathways control amyloid polymorphism and properties. *Biochemistry* 51, 2706−2716.

(10) Root, B. C., Pellegrino, L. D., Crawford, E. D., Kokona, B., and Fairman, R. (2009) Design of a heterotetrameric coiled coil. *Protein Sci.* 18, 329−336.

(11) Chen, S., and Wetzel, R. (2001) Solubilization and disaggregation of polyglutamine peptides. *Protein Sci.* 10, 887−891.

(12) Crestfield, A. M., Moore, S., and Stein, W. H. (1963) The preparation and enzymatic hydrolysis of reduced and S-carboxymethylated proteins. *J. Biol. Chem.* 238, 622−627.

(13) Rosen, H. (1957) A modified ninhydrin colorimetric analysis for amino acids. *Arch. Biochem. Biophys.* 67, 10−15.

(14) Pace, C. N., Vajdos, F., Fee, L., Grimsley, G., and Gray, T. (1995) How to measure and predict the molar absorption coefficient of a protein. *Protein Sci.* 4, 2411−2423.

(15) Venyaminov, S., and Kalnin, N. N. (1990) Quantitative IR spectrophotometry of peptide compounds in water ($H_2O$) solutions. I. Spectral parameters of amino acid residue absorption bands. *Biopolymers* 30, 1243−1257.

(16) Jackson, M., and Mantsch, H. H. (1995) The use and misuse of FTIR spectroscopy in the determination of protein structure. *Crit. Rev. Biochem. Mol. Biol.* 30, 95−120.

(17) Biancalana, M., Makabe, K., Koide, A., and Koide, S. (2009) Molecular mechanism of thioflavin-T binding to the surface of beta-rich peptide self-assemblies. *J. Mol. Biol.* 385, 1052−1063.

(18) Mok, Y. F., Ryan, T. M., Yang, S., Hatters, D. M., Howlett, G. J., and Griffin, M. D. (2011) Sedimentation velocity analysis of amyloid oligomers and fibrils using fluorescence detection. *Methods* 54, 67−75.

(19) Smith, M. H., Miles, T. F., Sheehan, M., Alfieri, K. N., Kokona, B., and Fairman, R. (2010) Polyglutamine fibrils are formed using a simple designed beta-hairpin model. *Proteins* 78, 1971−1979.

(20) Rigotti, D. J., Kokona, B., Horne, T., Acton, E. K., Lederman, C. D., Johnson, K. A., Manning, R. S., Kane, S. A., Smith, W. F., and Fairman, R. (2005) Quantitative atomic force microscopy image analysis of unusual filaments formed by the *Acanthamoeba castellanii* myosin II rod domain. *Anal. Biochem.* 346, 189−200.

(21) Jiao, Y., and Schaffer, T. E. (2004) Accurate height and volume measurements on soft samples with the atomic force microscope. *Langmuir* 20, 10038−10045.

(22) Knoll, A., Magerle, R., and Krausch, G. (2001) Tapping mode atomic force microscopy on polymers: where is the true sample surface? *Macromolecules* 34, 4159−4165.

(23) Nagarkar, R. P., Hule, R. A., Pochan, D. J., and Schneider, J. P. (2008) *De novo* design of strand-swapped beta-hairpin hydrogels. *J. Am. Chem. Soc.* 130, 4466−4474.

(24) Thakur, A. K., and Wetzel, R. (2002) Mutational analysis of the structural organization of polyglutamine aggregates. *Proc. Natl. Acad. Sci. U.S.A. 76* 99, 17014−17019.

(25) Volpatti, L. R., Vendruscolo, M., Dobson, C. M., and Knowles, T. P. (2013) A clear view of polymorphism, twist, and chirality in amyloid fibril formation. *ACS Nano* 7, 10443−10448.

(26) Walters, R. H., and Murphy, R. M. (2009) Examining polyglutamine peptide length: a connection between collapsed conformations and increased aggregation. *J. Mol. Biol.* 393, 978−992.

(27) Schneider, R., Schumacher, M. C., Mueller, H., Nand, D., Klaukien, V., Heise, H., Riedel, D., Wolf, G., Behrmann, E., Raunser, S., Seidel, R., Engelhard, M., and Baldus, M. (2011) Structural characterization of polyglutamine fibrils by solid-state NMR spectroscopy. *J. Mol. Biol.* 412, 121−136.

(28) Kokona, B., Rosenthal, Z. P., and Fairman, R. (2014) The role of the coiled-coil structural motif in polyglutamine aggregation. *Biochemistry*, in press DOI: 10.1021/bi500449a.